In-house low-resolution X-ray crystallography

Gwyndaf Evans,* Pietro Roversi
and Gérard Bricogne

MRC Laboratory of Molecular Biology, Hills
Road, Cambridge CB2 2QH, England

Correspondence e-mail:
gwyndaf@mrc-lmb.cam.ac.uk

It is demonstrated that standard in-house protein crystal X-ray diffraction apparatus can be used to measure very low resolution reflections with only a few modifications. The apparatus and modifications are described in detail and tested on two different macromolecular crystal samples: lysozyme and the 30S ribosomal subunit. Contrast-variation measurements on tetragonal hen egg-white lysozyme demonstrate the potential usefulness of the apparatus in providing accurate data for the determination of macromolecular envelopes. In contrast, the measurement of very low resolution diffraction from crystals of the 30S ribosome subunit illustrates how in-house facilities can provide data from small weakly diffracting crystals of a very large macromolecule.

1. Introduction

A common property shared by all protein crystals is their biphasic nature (Bernal & Crowfoot, 1934). That is, each unit cell consists of one or more ordered protein molecules surrounded by a highly disordered solvent region. The solvent typically consists of water, buffer and salt molecules and sometimes cryo-protectant molecules. The boundary between protein and solvent is typically fairly well defined and usually extends across a hydration layer only a few ångströms deep (Svergun *et al.*, 1998). This boundary may be represented in terms of a surface or envelope which describes the three-dimensional shape of a protein molecule. Inside this envelope, atoms are assumed to be ordered and to contribute to diffraction intensities at high resolution. Outside the envelope, atoms are disordered and difficult to model as a large number of single atoms with individual positional and thermal displacement parameters. This region is, therefore, normally assumed to have a constant electron density and a high temperature factor and thus to contribute only to low-resolution diffraction intensities.

Research into the determination of the protein envelope in a crystal using X-ray diffraction started with the work of Bragg & Perutz (1952). A few years earlier, Boyes-Watson *et al.* (1947) had already observed that substitution of ammonium sulfate for water as the solvent in crystals of horse methaemoglobin lowered the intensities of low-order reflections but left higher order intensities unchanged. These changes were interpreted as being a consequence of variation of the mean electron density of the solvent surrounding the protein molecules under the assumption that the protein molecules themselves were being left unchanged. By making diffraction intensity measurements under five different conditions corresponding to a salt-free solvent and four different salt concentrations, Bragg & Perutz (1952) were able

to deduce an approximate form and size for the haemoglobin molecule.

This was the first example of the X-ray contrast-variation technique for the determination of protein envelopes. Since then, efforts have been made to determine more detailed envelopes using solvent-contrast effects (Carter *et al.*, 1990; Carter, 1998), the related technique of multiwavelength anomalous solvent contrast (MASC; Ramin *et al.*, 1999; Fourme *et al.*, 1995) and direct phasing approaches (Lunin *et al.*, 1998; Subbiah, 1991). These methods attempt to extract the information describing the form of the protein envelope from diffraction intensities at low resolution ($d_h > 10$ Å). Apart from a small number of exceptions, the measurement of these low-resolution data has been neglected for many years. The reason for this is partly that the effects of bulk solvent on low-resolution data (Phillips, 1980) has been neglected in crystallographic software until recently (Jiang & Brünger, 1994) and partly because in the everyday job of determining protein crystal structures by well established methods such as MIR(AS), SIR(AS), MR and MAD[1] low-resolution data are not always thought to be essential. Typical protein diffraction data sets will extend only as low as 20 Å resolution and in the worst cases these data may be saturated on the detector or corrupted by the presence of a poorly positioned or poorly designed beamstop. The lowest order reflections are almost never measured and thus are rarely exploited in terms of their usefulness in describing the molecular envelope.

A notable exception is the work of Harrison & Jack (1975), where signs and phases from small-angle X-ray scattering and very low resolution X-ray crystal diffraction (Harrison, 1969) and a 28 Å electron microscopy (EM) reconstruction (Jack *et al.*, 1975) were used to determine the positions of clusters of $PtCl_6^{2-}$ ions in crystals of tomato bushy stunt virus. Indeed, the combination of EM and X-ray crystallography is a recurring theme in both virus work (Prasad *et al.*, 1999; Wynne *et al.*, 1999; Dokland *et al.*, 1998; Simpson *et al.*, 1998; Grimes *et al.*, 1997; Rayment *et al.*, 1982) and in the determination of very large macromolecule structures (Harms *et al.*, 1999; Ban *et al.*, 1998; Glykos *et al.*, 1998; Wang *et al.*, 1997). In most cases, EM phases are used either to initiate or corroborate crystal structure solution. However, problems arise in the combination of EM and X-ray observations, since there is typically only a small range of resolution over which the two sources of information overlap. EM reconstructions are only usually informative to resolutions where $d_h > 15$ Å with very few exceptions, the most notable being the 7.4 Å reconstruction of the core protein of hepatitis B virus (Böttcher *et al.*, 1997). X-ray data, on the other hand, rarely extend into the low-resolution region. There exists, therefore, an unfulfilled need for the routine measurement of very low resolution diffraction data from macromolecular crystals as a first step towards extending the region of overlap between the EM and X-ray data.

---

[1] Abbreviations used: MIR(AS), multiple isomorphous replacement (with anomalous scattering); SIR(AS), single isomorphous replacement (with anomalous scattering; MR, molecular replacement; MAD, multiple wavelength anomalous diffraction.

The measurement of very low resolution data is usually associated with the use of synchroton radiation because of the good intrinsic collimation of the X-rays. Indeed, specialist facilities for the measurement of low-resolution X-ray crystal diffraction data are now being established (Tsuruta *et al.*, 1998). However, there still exists a preference by many experimenters towards measuring data in the home laboratory, as access to synchrotrons can still be restricted and involve delays of many months. Very low order reflections typically produce the strongest intensities, sometimes orders of magnitude stronger that the average intensities of reflections measured between 10 and 2 Å. This makes the very low order reflections accessible to measurement using conventional sources, even from relatively weakly diffracting crystals. Miller *et al.* (1999) have measured very low resolution reflections from poliovirus crystals using a rotating anode and a MAR 345 detection system. They collimated the X-ray beam using a 'pinhole' to produce a fine X-ray beam with an inevitable reduction in the X-ray flux incident on the sample. With this configuration, the lowest order reflections were measurable using exposure times as low as 15 s. Indeed, some of the earliest experiments referred to above were performed in-house on conventional sources and best demonstrate the possibilities if care is taken with instrumental design and set-up (Harrison, 1968; Perutz & Rogers, 1946).

In this paper, we present a modified X-ray diffraction camera which allows the accurate measurement of very low resolution reflections corresponding to Bragg spacings of 200 Å or greater using a conventional rotating-anode source and a commercial image-plate system while avoiding any significant loss in X-ray flux.

2. Experimental apparatus

2.1. Requirements of the experiment

Setting up a low-angle X-ray camera requires the removal of as much low-angle scattered radiation as possible, the aim being to minimize the level of X-ray background recorded on an area detector and ideally to make the background smoothly varying. Possible sources of unwanted background arise from (i) scatter caused by the interaction of the main X-ray beam with air before and after the specimen, (ii) scatter from collimating slits, (iii) scatter from filters and windows and (iv) scatter from disordered regions of the specimen itself including bulk solvent, the accompanying solvent surrounding the crystal and the loop material. We consider here only sources of scatter from the apparatus itself and will neglect the specimen as a source of contaminating scattering.

A fundamental principle in the design of low-angle X-ray cameras is the positioning of collimating slits sufficiently far upstream of the sample so that the scatter produced by those slits is suffciently well separated from the main beam path so as to allow its removal by a guard aperture positioned just before the sample (Huxley, 1953; Bolduan & Bear, 1949). We have attempted to use this idea and a helium-filled path to

reduce the above-mentioned sources of background as much as possible.

Most crystal diffraction cameras use a beamstop mounted as close to the crystal as possible so that air scatter is reduced without obscuring too much low-resolution data. Even so, data below 15 Å are typically missing or corrupted as a result of the finite size of the sample crystal. Reflections recorded on the detector surface within the penumbra of the beamstop shadow are systematically wrong because they are a result of diffraction from only a fraction of the total diffracting volume of the sample (see Fig. 3 in Carter, 1998). For this reason, the use of a beamstop position as close to the detector as possible is favoured. This in turn, however, forces the use of an evacuated beam path or alternatively a helium-filled air path between sample and detector.

2.2. Realisation of the requirements

The X-ray source used in this work was an Elliot GX-13 rotating anode with a foreshortened X-ray source size of 100×100 µm. Fig. 1 is a schematic diagram illustrating the diffraction camera downstream of the X-ray source. The generated X-rays are focused horizontally and vertically by 60 mm bent mirrors (Charles Supper Company, Natick, MA, USA). The mirror pair is immediately followed by a set of vertical and horizontal slits (S0) and then a 300 mm MAR imaging plate and standard base. The MAR system consists of a collimator assembly, sample-rotation axis, beamstop mount and translatable detector all mounted on an adjustable base allowing alignment into the X-ray beam. The collimator assembly houses two sets of vertical and horizontal slits positioned 110 mm (S1 in Fig. 1) and 60 mm (S2 in Fig. 1) upstream of the sample position. Each vertical and horizontal slit pair is followed by an ionization chamber which helps in base alignment. Just upstream of the sample is a removable collimator nose-piece designed to remove scatter introduced
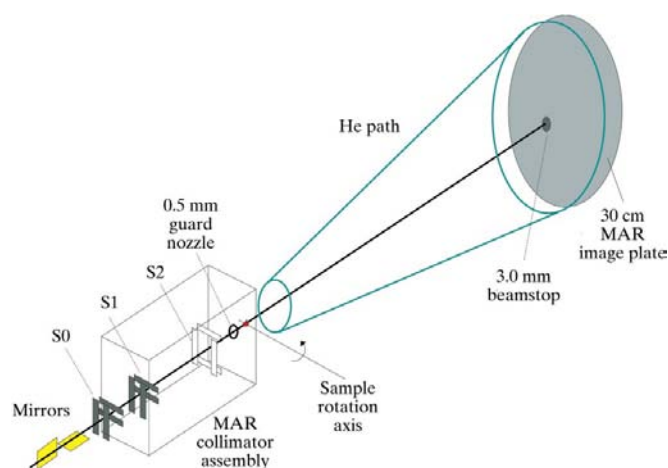
by the slits and air path within the collimator assembly. Nose-piece aperture diameters of 1.0, 1.5 and 2.0 mm are available with the detector; however, for this work a set of smaller diameter apertures were used, the smallest having a diameter of 0.5 mm. Alignment of the small aperture nose pieces with respect to the collimator slits was performed using an ionization chamber to monitor the flux exiting the collimator with and without the nose-piece in place. S1 and S2 slit openings of 0.25 mm vertically and horizontally were used during alignment, although during the measurement of low-resolution data slit S2 was opened fully and essentially excluded from the experiment.

The helium-filled flight path was constructed out of a transparent plastic bag which had been cut to shape and then heat sealed to form a cone. This bag was held at both ends by two flanges, one of 300 mm diameter at the detector side and one of 150 mm diameter near the sample. A small plastic funnel was cut to form a cone and then mounted onto the smaller flange to taper the helium path down to form an entrance window aperture of 15 mm in diameter. A 3 µm thick mylar window was placed over the entrance aperture and held in place with vacuum grease. The exit window was a 20 µm mylar film and had a 3 mm diameter beamstop glued to its centre on the inside surface. The beamstop was made by turning out a 3.0 mm diameter and 5 mm long aluminium rod and filling it with lead–tin solder. It was fixed to the He path window using Loctite Superglue. Adjustment of the path and beamstop position was made manually by loosening set screws which fixed the path to the MAR detector base and recording positions relative to the base using callipers. The front window of the path was placed as close to the sample position as possible without interfering with the nitrogen and dry air gas stream cooling the crystal. In the early stages of flooding the path with helium, the front mylar window acted as a moisture trap owing to its proximity to the Cryostream and some ice formation on the inside of the window was observed. Once all moisture in the path had been replaced, however, this problem no longer arose.

Fig. 2 shows the positions of each element of the diffraction camera relative to the source. The 100 mm space between the last defining slit and the nose-piece just before crystal is essential for producing a clean X-ray beam free of contaminating scatter. Fig. 2 illustrates this point. After being focused by the mirrors and collimated by slits S0 and S1, the main X-ray beam passes uninterrupted through the nose-piece onto the sample and then through the He path until it is absorbed by the beamstop. The size and alignment of the nose-piece is critical, since any interaction of the X-ray beam with the nose-piece would cause significant scatter into the low-resolution X-ray pattern. The aperture diameter must be large enough to allow the main beam through and small enough to confine any scatter produced by S1 to the beamstop. The sizes of the slits S0 and S1 were 0.4 and 0.35 mm, respectively, in both horizontal and vertical directions. The X-ray flux measured at the sample was comparable with the flux measured during normal operation of the camera using similar settings for both pairs of slits in the MAR collimator assembly. The relatively poor

Figure 1
Schematic overview of the diffraction camera used for the low-resolution measurements. From left to right are the Supper mirrors (Charles Supper) and mirror exit slits, S0, the MAR collimator front set of slits, S1, a modified collimator nose-piece or guard nozzle, the sample position, helium flight tube, beamstop and image-plate detector.

calibration of slits in this setup meant that the process of producing a clean X-ray camera free of excess background and slit scatter was an iterative process relying on observation as well as careful adjustment of apertures. Consequently, alignment can take as much as a day, as one relies completely on viewing detector images of the camera scatter. Better calibrated apertures would speed up this process by improving control over the experimental geometry.

3. Test case I: tetragonal hen egg-white lysozyme

To investigate the X-ray camera's suitability for performing contrast-variation experiments, we conducted experiments using the tetragonal form of hen egg-white lysozyme (HEWL). HEWL acts as a sufficiently robust and reproducible sample with which to perform test studies. It crystallizes readily even in the presence of cryo-protectant and its size and morphology can be controlled (Forsythe *et al.*, 1999) to produce test samples which emulate conditions potentially experienced in 'real life'.

3.1. Sample preparation

The crystals used in this study were grown from 1.5 M NaCl, 25% ethylene glycol and 0.1 M sodium acetate pH 4.7. In order to measure solvent-contrast effects, the crystals were soaked just prior to freezing in the Oxford Cryosystems Cryostream in two solutions (hereafter referred to as low and high density) having different electron densities. Although the crystals had been grown in the presence of a relatively low electron density solution, it was necessary to re-soak for 30 s in a better defined low-density solution so that an accurate estimate of the mean solvent electron density, ρ_s, in the crystal could be made. The low-density solution was 2 M NaCl, 25%

ethylene glycol and 0.1 M sodium acetate at pH 4.7 having $\rho_s = 0.349$ e Å^{-3}. A higher salt concentration was used in this case to stabilize the crystals in the absence of protein in solution.

The high-density crystals were obtained by soaking in a solution containing 2 M NaCl, 2 M D-glucose and 0.1 M sodium acetate pH 4.7 ($\rho_s = 0.391$ e Å^{-3}). High concentrations of D-glucose have previously been used by Yu & Caspar (1998) in the measurement of cubic insulin diffraction data. As well as increasing the mean electron density of the solvent, the glucose also acted as a cryo-protectant.

The mean electron densities of the soaking solutions were determined by careful volume and weight measurements of

Figure 3
Structure-factor amplitudes for HEW lysozyme's 18 lowest resolution reflections (56–35 Å) plotted for each of the six data sets. The diagram illutrates the high level of consistency between the three low-density data sets (1 to 3) even at the level of a single observation. Good consistency is seen also between data sets 4 and 6 with set 5 (dashed) appearing as an outlier at very low resolution.
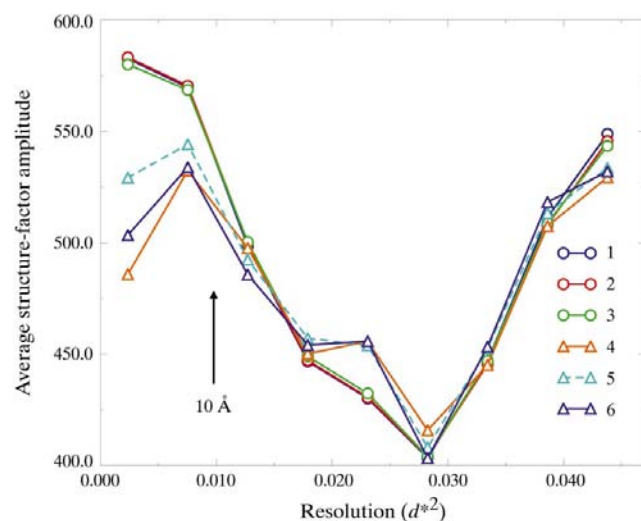
Figure 4
The binned average structure-factor amplitudes for all data (56–4.59 Å) plotted for the six HEWL data sets. The potential outlier data set 5 is shown dashed.
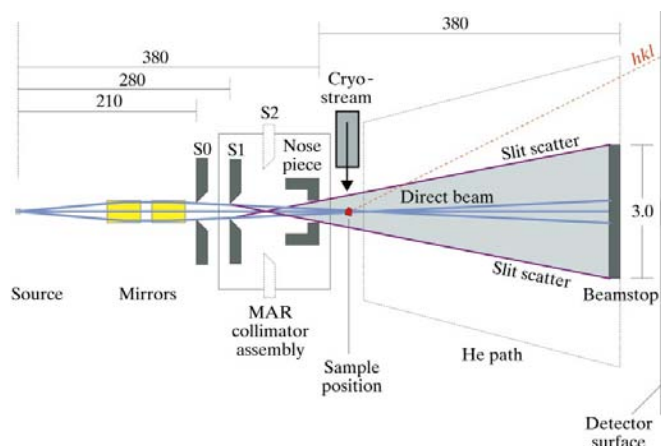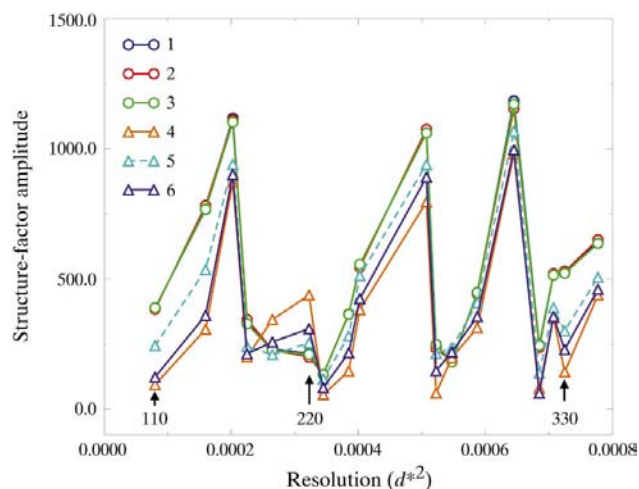
Figure 2
Illustration of the geometry of the low-resolution diffraction camera. Dimensions are in mm. (For clarity, the scale is expanded in the vertical direction by a factor of about 70 relative to the horizontal.) The collimating slits $S0$ and $S1$ act as a source of unwanted scattered radiation which can appear as linear streaks extending into the diffraction pattern outwards from the beam centre. This scatter is confined to lie inside the area obscured by the beamstop (shaded area) by the use of a guard aperture, in this case a modified collimator nose piece. Low-resolution diffracted X-rays (shown in red labelled *hkl*) pass through the He path and are incident on the detector surface.

Table 1
HEWL crystal and data-collection parameters and the results of data analysis using *MOSFLM* and *SCALA*.

Crystal and data-collection parameters.

Space group	$P4_32_12$
Resolution (Å)	56.0–4.59
Exposure time (min)	3–20
Oscillation angle (°)	3 (4 for crystal 5)
Total rotation range (°)	200–360
Solvent electron density ρ_s (Å^{-3})	0.349 (crystal 1, 2 and 3)
Solvent electron density ρ_s (Å^{-3})	0.391 (crystal 4, 5 and 6)

Summary of results.

Crystal	$a = b$ (Å)	c (Å)	Mosaicity (°)	Multiplicity	Completeness (%)	R_{merge}
1	78.81	36.80	0.2	19.1	100	3.4
2	78.76	36.79	0.2	13.2	100	4.3
3	78.78	36.84	0.2	24.3	100	3.1
4	78.11	37.51	0.3	23.9	100	4.4
5	78.12	37.10	0.9	13.1	100	5.3
6	77.72	37.24	0.3	16.2	100	3.4

the substances used in preparing the solution. This included making a record of the total amount of water added to the solutions to make up final volumes. It is estimated that the values of ρ_s given above are measured to better than 0.5%. It is highly unlikely that better accuracy is necessary given that the bulk-solvent density may differ from that of the prepared solutions because of protein boundary effects and/or incomplete penetration of the solution into the crystal.

The soaking times used for the high-density crystals were of the order of 1–2 min. The length of soak was based on observation of the crystal integrity. The crystals were not particularly stable in the high-density solution and in some cases crystals cracked owing to osmotic shock.

3.2. Measurement of diffraction data

The lowest resolution reflection from this tetragonal form of lysozyme appears at a resolution of about 56 Å. At a sample-to-detector distance of 425 mm the edge of the detector corresponded to a high-resolution limit of 4.58 Å. The beam path was flooded with helium and a 0.58 mm diameter nosepiece was inserted into the collimator end. At this stage some scatter was observed at resolutions with $d_\mathbf{h} > 100$ Å but this was acceptable as it did not interfere with the low-resolution reflections or surrounding background. Data were recorded from a total of six crystals: three at low density and three at high density. The crystals were frozen directly into a nitrogen Cryostream operating at 100 K. The data-collection parameters and results of analysis with *MOSFLM* (Leslie, 1992) and *SCALA* (Collaborative Computational Project, Number 4, 1994) are shown in Table 1. In all cases an oscillation range of 3° was used, except for crystal 5 where 4° oscillations were used. The total rotation range used varied but in each case all the data between 56 and 4.59 Å were measured with average multiplicities greater than 13.

A consistent decrease of 0.7–1.1 Å in the *a* and *b* axes was observed for the high-density crystals relative to the low-density crystals. Similarly, the *c* axis was found to increase by 0.3–0.7 Å. The mosaicities of the low-density crystals were estimated to be about 0.2°. The high-density crystals had consistently higher mosaicity but crystal 5 appeared to be an outlier among the six crystals with an estimated mosaicity of 0.9°. The higher than average R_{merge} (see Table 1) also indicates that the crystal may not have been of as high a quality as the other five.

3.3. Scaling

The six data sets were placed on a common scale using *SCALEIT* (Collaborative Computational Project, Number 4, 1994). The scaling was performed using data between 10 and 4.59 Å under the assumption that the expected contrast-variation effects are negligible for resolutions higher that 10 Å and that the non-isomorphism was not significant at 4.59 Å. This strategy has been verified using synthetic data generated for tetragonal HEWL with four different mean solvent electron densities (unpublished results). However, no attempt has been made to model the effects of non-isomorphism on the scaling procedure. At low resolution, changes in structure-factor amplitudes owing to non-isomorphism can be expected to be small relative to the changes observed owing to contrast variation. However, the reliance upon high-resolution data for scaling imposes requirements on the level of acceptable non-isomorphism. This is evidently where the advantage of the MASC technique lies.

A further complication in contrast variation relates to the handling of the significant changes in sample absorption one can expect when the mean electron density of the solvent in and around the crystal sample is changed significantly. In the present study this difficulty has been overcome by relying upon high multiplicity of measurement and spherical harmonic secondary beam-scaling corrections implemented by Phil Evans in *SCALA*. Low values of R_{merge} over all resolution ranges are indicative of the success of this procedure.

3.4. Observation of contrast variation

Figs. 3 and 4 show the effect on the low-resolution data of varying the solvent electron density. In Fig. 3 structure-factor amplitudes are plotted for data between 56 and 15 Å. The low contrast data sets agree to within a few percent demonstrating that data from different (but isomorphous) crystals can be recorded accurately and scaled together using only data between 10 and 4.59 Å, while maintaining the correct relative scale at low resolution. The high-density data sets (4–6) are less well behaved, however, with data set 5 emerging as an outlier among the three data sets. The effects of the change in solvent electron density are clearly visible in Fig. 4. Below about 10 Å the magnitudes of the average structure factors between low- and high-density data sets diverge to the point where they differ by about 20%. Apart from a glitch at 6.6 Å, the agreement between the average structure factors for all data sets at higher resolutions is within 4%.

Variation in the observed structure factors between the three high-density crystals could also be a consequence of small variations in the soaking times of the three crystals. No systematic behaviour was observed as a result; however, the effect of soaking time will form part of further studies into contrast-variation effects.

The effect of the contrast variation can be observed directly in the diffraction patterns from the low- and high-density crystals of HEWL. Fig. 5 shows regions of two 12° overlay images from crystal 1 (low density) and crystal 6 (high density). In both cases, the 110, 220 and 330 reflections are
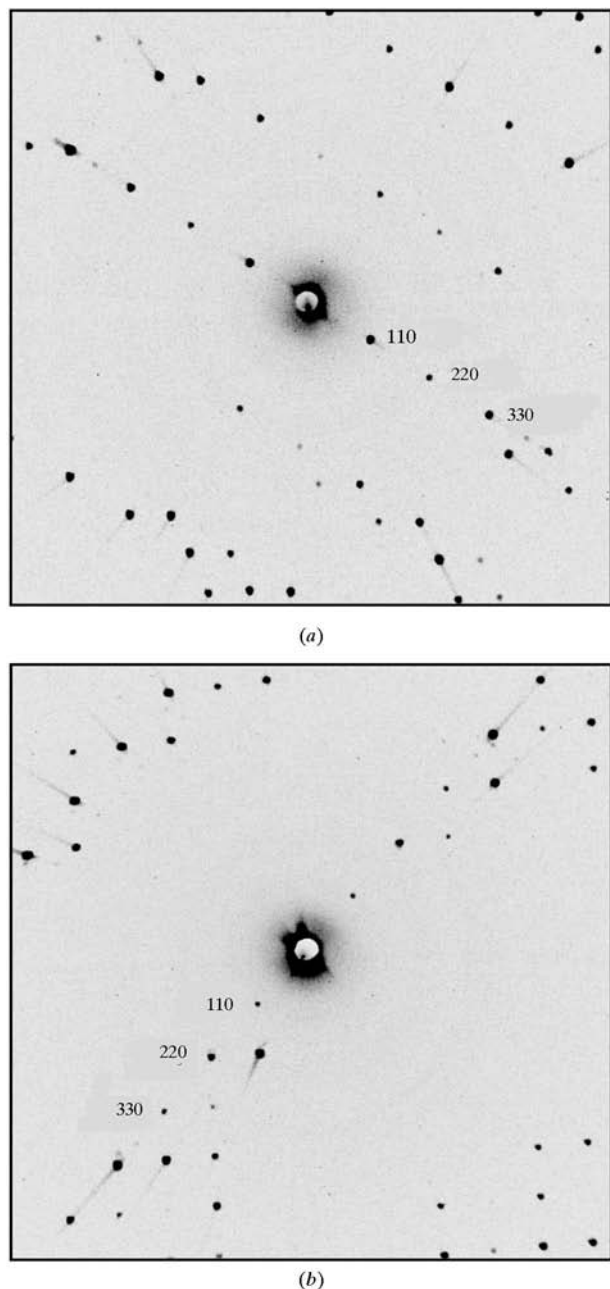

(a)

(b)

Figure 5
Two 12° overlay images showing the region of reciprocal space from tetragonal HEWL crystals containing the 110, 220 and 330 reflections from (a) crystal 1 having ρ_s = 0.349 and (b) crystal 6 having ρ_s = 0.391.

Table 2
30S ribosomal subunit crystal and data-collection parameters and the results of data analysis using *MOSFLM* and *SCALA*.

Crystal and data-collection parameters.

Space group	$P4_12_12$
Unit-cell parameters (Å)	401.5 × 401.5 × 174.5
Sample dimensions (µm)	200 × 80 × 80
Resolution (Å)	180–18
Exposure time (min)	10
Oscillation angle (°)	1
Total rotation range (°)	145

Summary of results.

Resolution (Å)	No. measured	No. unique	Multiplicity	Completeness (%)	R_{merge}
56.92	439	61	7.2	93.8	0.027
40.25	896	99	9.1	100.0	0.029
32.86	1170	123	9.5	100.0	0.041
28.46	1359	134	10.1	100.0	0.053
25.46	1569	153	10.3	100.0	0.073
23.24	1770	173	10.2	100.0	0.091
21.51	1790	173	10.3	100.0	0.126
20.12	1996	189	10.6	100.0	0.188
18.97	2073	200	10.4	100.0	0.260
18.00	2214	210	10.5	100.0	0.299
Total	15275	1513	10.1	99.7	0.057

visible and are labelled. Although the images are not on the same relative scale, one can still clearly observe changes in the intensities of the 110, 220 and 330 reflections which are, respectively, large, small and large in the low-density crystal, and small, large and small in the high-density crystal. This corresponds to the intensity changes observed and labelled in Fig. 3.

4. Test case II: 30S ribosome

The structure of a bacterial 30S ribosomal subunit was solved to 5.5 Å resolution by Clemons *et al.* (1999). It crystallizes in the tetragonal space group $P4_12_12$, with approximate unit-cell parameters $a = b = 401.5$, $c = 174.5$ Å. The crystal used for this study was approximately 200 × 80 × 80 µm in size and was frozen to 100 K. To reduce further the scatter in the very low resolution part of the diffraction pattern the MAR collimator assembly was also flooded with helium. This produced a clean diffraction camera down to about 250 Å.

Data-collection parameters and results of analysis are given in Table 2. The data are complete and highly redundant, apart from four reflections in the lowest resolution bin which were not present in the final merged data set. The high quality of the results suggests that the data were free from the effects of corruption discussed in §2.1. On inspection, it turned out that three of the four missing reflections had been rejected at the integration stage because they were saturated on the detector. These were the 200, 101 and 220 and their symmetry-related reflections. The 110 reflection and its symmetry mates had been excluded because it was too close to the beamstop. This is summarized in Table 3. Fig. 6 shows zoomed regions of 1°

Table 3
The status of all reflections between 284 and 125 Å.

A tick mark indicates those reflections and symmetry mates that were succesfully integrated and scaled. OL indicates reflection that were overloaded or saturated on the detector.

Miller indices	Resolution (Å)	Measured?
110	283.9	Too close to beamstop
200	200.8	OL
210	179.6	√
101	160.0	OL
111	148.7	√
220	142.0	OL
201	132.0	√
310	127.0	√
211	125.1	√

images from the ribosome data where the 110 and 200 reflections are visible. The 110 reflection is just grazing the beamstop and has been rejected because it contains pixels which lie outside the defined active region of the detector (a 2.3 mm exclusion region was defined during integration with *MOSFLM*). It can be seen that although the 200 reflection has been rejected because it is saturated, it is nevertheless clearly resolved from its neighbouring reflections and from the beamstop. Similarly, the 101 and 220 reflections were well resolved but saturated. It is reasonable to assume that on remeasuring these reflections with a reduced exposure, integration would proceed normally.
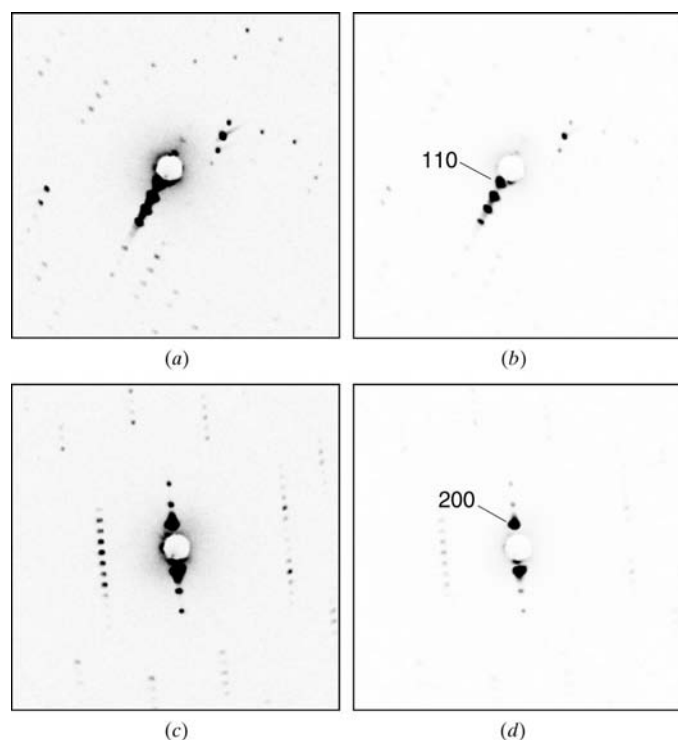

Figure 6
The central region of 1° rotation images of very low angle diffraction from a tetragonal crystal of the 30S ribosomal subunit. The images shown contain the 110 reflection at two contrast levels (*a* and *b*) and the 200 reflection (*c* and *d*) also at two contrast levels.

Similar problems were encountered by Miller *et al.* (1999) during the in-house measurement of poliovirus crystal diffraction data. A small number of very low resolution reflections needed to be remeasured at much reduced exposure levels. These measurements were made however at the expense of reflections which were present in the longer exposure data set. This meant that there were no common reflections in the high- and low-exposure data sets which could be used to scale the data sets together. Scaling was performed solely on the basis of the recorded exposure times under the assumption that the beam intensity and diffracting volume were constant. In our study, the low-exposure pass through the data was not performed, but it is believed that similar scaling problems would have been encountered.

5. Conclusions

High-quality low-resolution data can be measured in-house with only minor modifications to existing protein crystallography hardware. The results of the contrast-variation experiment demonstrate that such effects can be measured in a straightforward way without the need for extraordinary apparatus or a synchrotron. Because the low-order reflections required in these methods are orders of magnitude stronger than the higher order reflections typically recorded by crystallographers, the measurements are particularly suited to in-house X-ray sources, which are in turn orders of magnitude weaker than synchrotron sources. The case of MASC, however, is an obvious exception because a tunable source of X-rays is an absolute prerequisite.

The rapid measurement of very low resolution diffraction data from crystals of the 30S ribosome has a number of implications. Firstly, the apparatus can allow convenient and quick screening of crystal diffraction at very low resolution which can be useful during the early stages of improvement of crystal-growth conditions where no high-angle diffraction is visible. More obviously, because many synchrotron beamlines are not permanently set up to measure very low resolution data, in-house measurements can potentially save on the use of synchrotron beam time.

We believe that the combination of routine in-house low-resolution data collection and existing contrast-variation data-analysis techniques, as well as those that will appear in the next few years, will lead to a straightforward method for the determination of the protein envelope.

References

Ban, N., Freeborn, B., Nissen, P., Penczek, P., Grassucci, R. A., Sweet, R., Frank, K., Moore, P. B. & Steitz, T. A. (1998). *Cell*, **93**, 1105–1115.
Bernal, J. & Crowfoot, D. (1934). *Nature (London)*, **133**, 794–795.

Bolduan, O. E. A. & Bear, R. S. (1949). *J. Appl. Phys.* **20**, 983–992.

Böttcher, B., Wynne, S. A. & Crowther, R. T. (1997). *Nature (London)*, **386**, 88–91.

Boyes-Watson, J., Davidson, E. & Perutz, M. F. (1947). *Proc. R. Soc. London Ser. A*, **191**, 83–132.

Bragg, W. L. & Perutz, M. F. (1952). *Acta Cryst.* **5**, 277–283.

Carter, C. W. Jr (1998). *Direct Methods for Solving Macromolecular Structures*, pp. 227–237. Netherlands: Kluwer Academic Publishers.

Carter, C. W. Jr, Crumley, K. V., Coleman, D. E., Hage, F. & Bricogne, G. (1990). *Acta Cryst.* A**46**, 57–68.

Clemons, W. M. Jr, May, J. L. C., Wimberly, B. T., McCutcheon, J. P., Capel, M. S. & Ramakrishnan, V. (1999). *Nature (London)*, **400**(6747), 833–840.

Collaborative Computational Project, Number 4 (1994). *Acta Cryst.* D**50**, 760–763.

Dokland, T., McKenna, R., Sherman, D. M., Bowman, B. R., Bean, W. F. & Rossmann, M. G. (1998). *Acta Cryst.* D**54**, 878–890.

Forsythe, E. L., Nadarajah, A. & Pusey, M. L. (1999). *Acta Cryst.* D**55**, 1005–1011.

Fourme, R., Shepard, W., Kahn, R., l'Hermite, G. & de La Sierra, I. L. (1995). *J. Synchrotron Rad.* **2**, 36–48.

Glykos, N. M., Holzenburg, A. & Phillips, S. E. (1998). *Acta Cryst.* D**54**, 215–225.

Grimes, J. M., Jakana, J., Ghosh, M., Basak, A. K., Roy, P., Chiu, W., Stuart, D. I. & Prasad, B. V. (1997). *Structure*, **5**, 885–893.

Harms, J., Tocilj, A., Levin, I., Agmon, I., Stark, H., Kolln, I., van Heel, M., Cuff, M., Schlunzen, F., Bashan, A., Franceschi, F. & Yonath, A. (1999). *Structure Fold. Des.* **7**(8), 931–941.

Harrison, S. C. (1969). *J. Mol. Biol.* **42**, 457–483.

Harrison, S. C. (1968). *J. Appl. Cryst.* **1**, 84–90.

Harrison, S. C. & Jack, A. (1975). *J. Mol. Biol.* **97**, 173–191.

Huxley, H. E. (1953). *Acta Cryst.* **6**, 457–465.

Jack, A., Harrison, S. C. & Crowther, R. A. (1975). *J. Mol. Biol.* **97**, 163–172.

Jiang, J. S. & Brunger, A. T. (1994). *J. Mol. Biol.* **243**(1), 100–115.

Leslie, A. G. W. (1992). *Jnt CCP4/ESF–EAMCB Newslett. Protein Crystallogr.* **26**.

Lunin, V., Lunina, N., Petrova, T., Urzhumtsev, A. & Podjarny, A. (1998). *Acta Cryst.* D**54**(5), 726–734.

Miller, S. T., Genova, J. D. & Hogle, J. M. (1999). *J. Appl. Cryst.* **32**, 1183–1185.

Perutz, M. F. & Rogers, G. L. (1946). *J. Sci. Instrum.* **23**(9), 217.

Phillips, S. E. V. (1980). *J. Mol. Biol.* **142**(4), 531–554.

Prasad, B. V., Hardy, M. E., Dokland, T., Bella, J., Rossmann, M. G. & Estes, M. K. (1999). *Science*, **286**, 287–290.

Ramin, M., Shepard, W., Fourme, R. & Kahn, R. (1999). *Acta Cryst.* D**55**, 157–167.

Rayment, I., Baker, T. S., Caspar, D. L. & Murakami, W. T. (1982). *Nature (London)*, **295**(5845), 110–115.

Simpson, A. A., Chipman, P. R., Baker, T. S., Tijssen, P. & Rossmann, M. G. (1998). *Structure*, **6**(11), 1355–1367.

Subbiah, S. (1991). *Science*, **252**, 128–133.

Svergun, D. I., Richard, S., Koch, M. H., Sayers, Z., Kuprin, S. & Zaccai, G. (1998). *Proc. Natl Acad. Sci. USA*, **95**(5), 2267–2272.

Tsuruta, H., Reddy, V. S., Wikoff, W. R. & Johnson, J. E. (1998). *J. Mol. Biol.* **284**(5), 1439–1452.

Wang, J., Hartling, J. A. & Flanagan, J. (1997). *Cell*, **91**, 447–456.

Wynne, S. A., Crowther, R. T. & Leslie, A. G. W. (1999). *Mol. Cell*, **3**, 771–780.

Yu, B. & Caspar, D. L. D. (1998). *Biophys. J.* **74**, 616–622.